Airborne Ionospheric Gradient Monitoring for Dual-Frequency GBAS

Daniel Gerbeth, Maria Caamano, *German Aerospace Center (DLR)*
Mihaela-Simona Circiu, *ESA/ESTEC*
Michael Felux, *Zurich University of Applied Sciences (ZHAW)*

BIOGRAPHIES

Daniel Gerbeth received a Bachelor and Master's degree in Electrical Engineering and Information Technology from Karlsruhe Institute of Technology, Germany in 2014. During Master studies he specialized in aerospace technology and navigation. After working in the field of sensor fusion and navigation aiding at Fraunhofer IOSB he joined German Aerospace Center (DLR) in May 2015 and is involved in the research on GBAS and reliable navigation for UAS since then.

Maria Caamano received a Master's degree in Telecommunications Engineering from the University of Oviedo, Spain, in March 2015. During Master studies, she specialized in the field of signal theory and communications. The same year she joined the German Aerospace Center (DLR), where she is working on the impact of ionospheric irregularities on GBAS.

Dr. Mihaela-Simona Circiu received a Bachelor and Master in Computer Engineering at Technical University Gheorghe Asachi, Romania and in 2012 she obtained a 2nd level Specialized Master in Navigation and Related Application from Politecnico di Torino, Italy. She holds a PhD in Electrical Engineering from RWTH Aachen, Germany. Between 2013-2021 she worked at the German Aerospace Center with focus on multi-frequency multi-constellation Ground Based Augmentation System. Since April 2021, she is working as contractor at European Space Agency, in the Netherlands, with focus on Galileo system performance.

Dr. Michael Felux received a diploma in Technical Mathematics from the Technical University of Munich in 2009 and a PhD in Aerospace Engineering in 2018. From 2009 to 2020 he worked on different aspects of aeronautical navigation, focusing mainly on GBAS. In April 2020 he joined the Zurich University of Applied Sciences where he is a Senior Lecturer for CNS/ATM and leading the Aeronautical Infrastructure group at the Center for Aviation.

ABSTRACT

Certified Ground Based Augmentation Systems (GBAS) as of today operate using only GPS signals in the L1 frequency band to enable precision approach guidance for landing aircraft. Ionospheric activity (i.e., scintillations and/or large abnormal ionospheric gradients) is a major limitation for the availability of current GBAS services, especially in equatorial and polar regions. To overcome these availability limitations, current developments aim at extending GBAS to the use of dual-frequency and multi-constellation (DFMC) techniques. Using signals on a second frequency, in this case L5/E5a, allows for a less conservative ionospheric monitoring, improving the availability of GBAS in regions with high ionospheric activity.
In previous work, we proposed an airborne ionospheric gradient monitoring concept to detect significant ionospheric delay differences between a GBAS ground station and an airborne user. This concept was initially developed for the assumption of a single satellite affected by an ionospheric gradient. While extending it for case with multiple satellites simultaneously affected, the proposed monitoring thresholds were getting extremely sensitive with a consequent raise of the false alarm probability of the monitor. Furthermore, the concurrent impact of an ionospheric gradient on multiple satellites could deteriorate the monitoring performance, and thus the detectability. In this work, we revisit the previously proposed monitoring scheme to improve its robustness, especially in the situation when several satellites are affected simultaneously. This is achieved through a median removal step, which makes the quantities derived from the pseudorange corrections from the ground station and the ionospheric delay estimates derived from dual-frequency pseudorange measurements from the aircraft comparable without adding a bias to the unaffected satellites. In addition, we propose a method to monitor all satellites currently in use at once, avoiding the need to make conservative assumptions about the maximum number of affected satellites.

INTRODUCTION

The Ground Based Augmentation System (GBAS) provides differential corrections and assures integrity of the navigation solution for aircraft flying precision approaches based on the use of Global Navigation Satellite Systems (GNSS). Operational GBAS ground stations today provide corrections for the L1 signals of GPS/GLONASS only. By design, GBAS generates corrections that are valid and accurate in the vicinity of the ground reference station. Nonetheless, a decorrelation of the ionospheric error typically occurs over distance and can lead to positioning errors of aircraft on approach [1] [2] [3]. This situation can become harmful in case of significant ionospheric activity, such as the presence of abnormally large ionospheric gradients acting between the GBAS station and the aircraft on approach. Thus, it is essential to conservatively bound the resulting errors which tends to lead to a decrease in availability, or to monitor for such potentially harmful ionospheric effects and prevent significant positioning errors while flying precision approaches. With the introduction of dual-frequency GNSS into GBAS planned for future GBAS approach service types (GAST) [4], new monitoring options arise and can be leveraged.

In previous work Felux et al. developed in [5] and validated in [6] a method to mitigate the threat of ionospheric gradients for single-frequency positioning by using the second available frequency for monitoring purposes. One of the main design drivers for new GBAS service types was to maintain backwards compatibility and use the existing VHF Data Broadcast (VDB) with its limited capacity [7]. Therefore, the ionospheric delays calculated at the ground station cannot be transmitted to the aircraft on approach, and, at the aircraft, only the pseudorange corrections are available. Thus, this dual-frequency ionospheric monitoring scheme combines pseudorange corrections from two different frequencies transmitted from the ground station to calculate a "pseudo" ionospheric delay from the ground station and compares these values with dual-frequency ionospheric delay estimations for each satellite computed at the aircraft. This allows individual satellites with significant errors to be excluded from further processing without additional (ionospheric) monitoring effort in the GBAS ground station.
Initially the concept was developed for a single affected satellite [8], and later it was extended for multiple satellites affected simultaneously [5]. However, to tackle the multiple satellites affected case, the monitor has to assume a certain number of satellites that could potentially be affected at the same time, which, a priori, is not known. Although for the case of a single constellation (GPS), this number is typically assumed to be two, the case for more constellations is not clear.
While for individual affected satellites, the previously described monitor can detect and exclude the affected satellite very reliably, the detectability deteriorates with an increasing number of satellites affected simultaneously, potentially leaving ionospheric gradients undetected. Furthermore, it could experience an excessive false alarm rate when assuming a high number of satellites simultaneously affected.

In this work, we revisit this previously proposed dual-frequency airborne ionospheric monitoring scheme for GBAS described in [5] to improve the robustness of the monitor especially when several satellites are affected by an ionospheric gradient. Based on the original monitoring concept, a new, bias-free test statistic is derived, which successfully removes effects of common biases on the ionospheric estimates (e.g. from a different set of satellites used on ground and airborne side or different instrumental delays on the L1 and L5 signals), improving detection capabilities further. Additionally, the method to build a combined test statistic for multiple affected satellites at once is refined and a new detection threshold is proposed.

In the following sections, we describe and validate three main updates to the previous concept:

- A new derivation of a bias-free test statistic describing the ionospheric difference between corrections and estimations at the airborne side.
- An updated version of the test, performed in position instead of range domain. Furthermore, this updated version uses a tighter bound of the threshold when applying the monitor to multiple potentially affected satellites at once.
- A new monitoring scheme to monitor all used satellites at once avoiding prior knowledge or assumptions on the number of simultaneously affected satellites

After introducing these updates, we compare the new and the previous approaches and show first results of the new monitoring performance in a simulated landing scenario with several satellites affected by an ionospheric gradient.

METHODS

This work is based on the ionospheric monitoring scheme presented previously ([5] [6]) and adjusts several aspects. The justifications behind the design of the initial concept is summarized here only very briefly. For further details on the steps taken in the development

of that monitoring scheme the interested reader is referred to the open access journal article [3] in which all steps are explained in detail.
The basic idea is to compare the ionospheric delay estimates at the ground station with the ionospheric delay estimates at the aircraft. In the airborne system the ionosphere for satellite i can be directly estimated using smoothed pseudoranges ($\hat{\rho}$) on two frequencies:

$$I_{air,i} = \frac{f_{L5}^2}{f_{L1}^2 - f_{L5}^2}\left(\hat{\rho}_{L5,i} - \hat{\rho}_{L1,i}\right) \tag{1}$$

with f_{L1} and f_{L5} being the center frequencies of the L1/E1 and L5/E5a GNSS signals. Other frequency combinations allow a similar estimation but we focus on using L5/E5a as second frequency available for aviation.
The ionospheric delays experienced at the GBAS ground station cannot be directly recovered from the corrections received by the aircraft. Smooth clock corrections and averaging steps in the PRC generation process remove all common ionospheric delays. Only a pseudo-ionospheric delay can therefore be derived:

$$I_{PRC,i} = \frac{f_{L5}^2}{f_{L1}^2 - f_{L5}^2}\left[\left(PRC_{L5,i} + \Delta t \cdot RRC_{L5,i}\right) - \left(PRC_{L1,i} + \Delta t \cdot RRC_{L1,i}\right)\right] \tag{2}$$

with PRC_i and RRC_i being the pseudorange and range-rate corrections on either L1/E1 or L5/E5a for satellite i and Δt the time difference between the current time of airborne measurement and the time of generation of the corrections.
Note that while the absolute ionospheric delays seen by the GBAS ground station cannot be recovered from the corrections, the relative ionospheric differences between all satellites are still preserved within $I_{PRC,i}$. Consequently, another step is required to make both values (equations (1) and (2)) comparable and allow testing for ionospheric gradients. In previous work, the mean values from all the airborne ionospheric estimates and the mean values from all the pseudo-iono delay estimates from the corrections were removed to achieve such comparable values. To avoid introducing biases that could deteriorate the performance of the monitoring, this process is refined in the current work as described in the following.

New Test Statistic

Our test statistic shall describe how much an ionospheric estimate differs from the ionospheric pattern common to air and ground for each individual satellite. Therefore, we search for the best alignment of $-I_{air}$ and I_{PRC} given the fact that both can have an arbitrary offset to each other (the minus sign results from the opposite sign of the corrections with respect to the actual ionospheric delays that the corrections should compensate). What is of interest are then the outliers to this alignment – those describe satellites with major differences in ionospheric delay. A simplified visualization of this process is depicted in *Figure 1*, showing $-I_{air}$ and I_{PRC} values for 7 satellites.

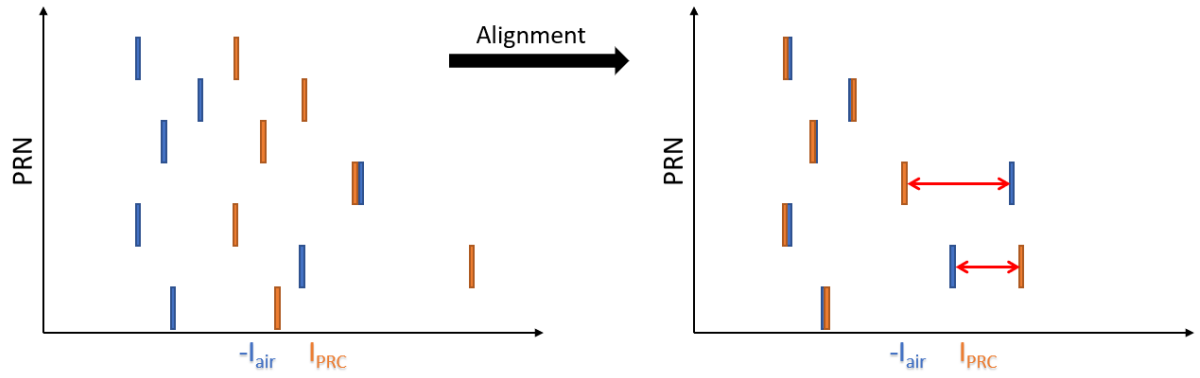

Figure 1 Visualization of the alignment process. Residual ionospheric differences are depicted in red in the right figure, showing the case of two simultaneously affected satellites.

What we consider best alignment is such that the total sum of all differences is smallest. Mathematically we are minimizing the L1 distance between the pseudo ionospheric delay estimates from the PRCs and the estimated ionospheric delays from the airborne

pseudorange measurements in the common set of satellites s_C. This minimum can be found when the median of the common set s_C is subtracted from the value of interest ($I_{air} + I_{PRC}$) for each satellite [9]. Therefore, the new test statistic for satellite i and frequency f is therefore calculated as:

$$I_{test,f,i} = I_{air,f,i} + I_{PRC,f,i} - median\left\{\left(I_{air,f,j} + I_{PRC,f,i}\right)_{j \in s_c}\right\} \tag{3}$$

This new estimator is bias free and preserves the actual ionospheric differences as long as not more than half of all satellites in the used subset are affected by an ionospheric gradient. Important to note here is that only satellites affected at either ground or airborne side are harmful. Depending on the distance to the airport, this leaves only a certain, limited area where a satellite could cause an unbound error. Considering the typical distribution of a constellation, the probability of more than half of the satellites affected can be considered almost negligible.

Now, within the pseudoranges and PRCs used in the derivation of the test statistic a number of biases (antenna biases, inter-frequency biases, …) can be present. Furthermore, the set of satellites used on ground potentially differs from the satellites used by an aircraft on approach. This would result in a common bias on all PRCs due to the smoothed clock adjustment process in the generation of the corrections [10]. Therefore, it is important that any of those biases do not directly affect the test statistic. Otherwise, such biases can potentially hide actual ionospheric differences in the test, while these could still influence single frequency positioning.
Fortunately, any biases (on any of the pseudoranges or corrections) common to all satellites are removed in the median removal step as can be seen in the following calculation.

With

$$f_{L1L5} = \frac{f_{L5}^2}{f_{L1}^2 - f_{L5}^2} \qquad P_{Lx} = PRC_{Lx,i} + \Delta t \cdot RRC_{Lx,i} \qquad m = median\left\{f_{L1L5} \cdot \left(\rho_{L5,j} - \rho_{L1,j}\right) + f_{L1L5} \cdot \left(P_{L5,j} - P_{L1,j}\right)\right\}_{j \in s_c}$$

we define:

$$I_{test,i} = f_{L1L5} \cdot \left(\rho_{L5,i} - \rho_{L1,i}\right) + f_{L1L5} \cdot \left(P_{L5,i} - P_{L1,i}\right) - m \tag{4}$$

A biased version of the test statistic for satellite i can be created by adding an individual bias (b_1 to b_4) to all of the pseudorange and correction terms:

$$I_{test,i}^b = f_{L1L5} \cdot \left((\rho_{L5,i} + b_1) - (\rho_{L1,i} + b_2) + \left(P_{L5,i} + b_3\right) - (P_{L1,i} + b_4)\right) - m \tag{5}$$

Reordering yields:

$$I_{test,i}^b = f_{L1L5} \cdot \left(\rho_{L5,i} - \rho_{L1,i} + P_{L5,i} - P_{L1,i}\right) + f_{L1L5} \cdot (b_1 - b_2 + b_3 - b_4) - m \tag{6}$$

where the two right summands are constant and can be considered a new constant bias term within the satellite specific delay estimate:

$$I_{test,i}^b = f_{L1L5} \cdot \left(\rho_{L5,i} - \rho_{L1,i} + P_{L5,i} - P_{L1,i}\right) + m' \tag{7}$$

Performing a median removal over all satellites on equation (7) yields exactly the unbiased I_{test} again, as m' is just a new common term among all test statistic.
While this property is helpful and removes all effects that are common to all satellites as well as differences between the used satellite sets on ground and in the airborne or at the two frequencies, it has to be mentioned that not all biases are mitigated from the test statistic like this. As recently also discussed in [11], some antenna and receiver dependent effects are specific to each satellite. Azimuth and elevation dependent antenna biases for example could hide existing gradients or vice versa lead to false alarms in geometry and antenna patters align unfavorable in weak geometries. Such effects are discussed again later and foreseen as core part of future work.

Definition of New Monitoring Condition

In the previous sections, we derived the updated test statistic and showed that it allows an unbiased estimation of the value of interest, the ionospheric delay difference between the ground reference station and an airborne GBAS user. From now on, we omit the frequency subscript f from equation (3) and continue using only L1/E1.

In previous work, we defined the test to check for harmful ionospheric gradients as follows:

$$\left|I_{test,i}\right| \leq \frac{E_{v,iono}}{\left|s_{vert,i}\right|} - 6.1 \cdot \sigma_{monitor,i} \tag{8}$$

A missed detection probability of 10^{-9} is attributed to the monitor in this case (i.e. 6.1 sigma), assuming that the noise in the test statistic follows a Gaussian distribution. The monitoring noise itself for satellite i consists of the noise and multipath contributions of both air ($\sigma^2_{air,L1}, \sigma^2_{air,L5}$) and ground ($\sigma^2_{gnd,L1}, \sigma^2_{gnd,L5}$) for the two used frequencies. These values are either transmitted by a GBAS station [12] in case of (σ^2_{gnd}) or defined in standards (σ^2_{air}) [13].

$$\sigma_{monitor,i} = \frac{f_{L5}^2}{f_{L1}^2 - f_{L5}^2}\sqrt{\sigma^2_{gnd,L1} + \sigma^2_{gnd,L5} + \sigma^2_{air,L1} + \sigma^2_{air,L5}} \tag{9}$$

The projection factor $s_{vert,i}$ describes the projection from range domain into the vertical axis of the position domain (in approach coordinates) and depends on the local satellite geometry and the glide path angle of the approach. $E_{v,iono}$ on the other hand, is a limit on the largest vertical position error due to an ionospheric anomaly. For brevity we skip the detailed derivations of both properties here, as their definition is no relevant for the further explanations. For details, please refer to [5].

Later in our previous paper, the test was conservatively extended for multiple (N) satellites as follows:

$$\sum_{i=1}^{N}\left|I_{test,i}\right| \leq \frac{E_{v,iono}}{\sum_{i=1}^{N}\left|s_{vert,i}\right|} - 6.1 \cdot \sqrt{\sum_{i=1}^{N}\sigma^2_{monitor,i}} \tag{10}$$

As monitoring takes place in range domain, the error limit in vertical $E_{v,iono}$ is scaled back into range domain by dividing it by the sum of all projection factors. This implies that the more satellites are considered to be simultaneously affected and not properly corrected by GBAS or already excluded by other monitoring, the more sensitive the monitor became up to a point where the monitoring would always trigger a false alarm.

However, instead of conservatively adding up all errors in range domain, we can make use of the knowledge of the geometry we have at the airborne user. Our previously defined test statistic in equation (3) describes the remaining ionospheric error (sign and magnitude) introduced into single frequency L1 positioning after applying the pseudorange corrections. In a similar manner as the GBAS protection levels are computed, we can now transfer our monitoring into position domain using the known projection factors (s) based on the satellite geometry.
Exemplary for the vertical domain, equation (10) becomes:

$$\left|\sum_{i=1}^{N}\left(I_{test,i} \cdot s_{vert,i}\right)\right| + 6.1 \cdot \sqrt{\sum_{i=1}^{N}\sigma^2_{monitor,i} \cdot s^2_{vert,i}} \leq E_{v,iono} \tag{11}$$

The core difference is that ionospheric induced errors in multiple satellites can compensate each other depending on the sign of the s-values. This significantly reduces the conservatism in the monitoring and reflects much more the actual situation and thereby, avoids that the left part of the equation grows extensively with every additional satellite added to the monitoring equation.
In fact, for N=1, i.e. a case of a single affected satellite, it is easy to see that both equations are equivalent. Furthermore, for N >1 it always holds that:

$$\left|\sum_{i=1}^{N}\left(I_{test,i} \cdot s_{vert,i}\right)\right| + 6.1 \cdot \sqrt{\sum_{i=1}^{N}\sigma^2_{monitor,i} \cdot s^2_{vert,i}} \leq \sum_{i=1}^{N}\left(\left|I_{test,i}\right| \cdot \left|s_{vert,i}\right|\right) + 6.1 \cdot \sqrt{\sum_{i=1}^{N}\sigma^2_{monitor,i} \cdot s^2_{vert,i}} \leq E_{v,iono} \tag{12}$$

The new monitoring condition is therefore always tighter or equal to the previous formulation. This allows avoiding strong assumptions on the number of simultaneously affected satellites, the major limitation of the previous monitoring concept. Furthermore, this opens up opportunities for new monitoring schemes, allowing for example monitoring the complete current set of common satellites (s_C) in a single test, simplifying monitoring logic and reducing computational effort significantly.

New Monitoring and Exclusion Strategy

After describing the basics on how to build and combine the refined test, a first proposal for a redefined monitoring scheme is given in this section. In previous work [5], the monitor was executed by comparing any n-satellite subset, being n the number of satellites assumed to be simultaneously affected, of the currently used satellites individually with the monitoring threshold. In this case n was assumed to be one, two, and up to the maximum number of satellites that where considered to be affected at once. Apart from the necessity of defining a maximum number of affected satellites, this additionally implied an increasing computational complexity when checking all 2, 3 or more satellites subsets out of the common used set. This is especially true for multi-constellation techniques where the number of possible subsets grows rapidly with the number of satellites available.

With the new monitoring equation and especially when looking at strong multi-constellation geometries, a different approach seems feasible, as we will verify later in the results. Instead of looking at cases of individual affected satellites, an airborne GBAS user can test whether equation (11) is fulfilled considering all currently used satellites.
If the threshold is not exceeded for this full common set, no ionospheric threat is considered present and no action is taken. Note that, in this case, an ionospheric gradient could be affecting several satellites, but still not be a threat for the aircraft position. Therefore, the current satellite set is continued to be used in single frequency positioning.
Otherwise, if the threshold is exceeded, a greedy exclusion algorithm is performed. Starting with the current set of N satellites, we built N individual subsets each with a different satellite excluded and recalculate the combined test statistic $\tilde{I}$ as:

$$\tilde{I}_{test,j} = \left| \sum_{\substack{i=1 \\ i \neq j}}^{N} \left(I_{test,i} \cdot s_{vert,i} \right) \right| + 6.1 \cdot \sqrt{\sum_{\substack{i=1 \\ i \neq j}}^{N} \sigma^2_{monitor,i} \cdot s^2_{vert,i}} \quad \forall\, j \in \{1 \dots N\} \tag{13}$$

Among all subsets we choose the one with the smallest combined test statistic $\tilde{I}_{test,j}$ to continue. If the threshold $E_{v,iono}$ is still exceeded, we use the current N-1 set and build all satellite subsets with a second satellite excluded, leaving N-2 satellites. The combined test statistic $\tilde{I}_{test,j}$ is recalculated again as shown above but for the remaining N-2 sets of N-2 satellites.
These steps are repeated until the current $\tilde{I}_{test,j}$ falls below the monitoring threshold, leaving us with a satellite subset where no significant ionospheric error remains present in the position domain. In case no such set can be found while we reach less than the minimum number of satellites required (i.e. 3 + the number of used constellations) we declare the system unavailable.

One important aspect to consider is that a passed test does not necessarily mean that no ionospheric differences are present or no gradient is effective. It might as well be that a satellite shows a significant difference, but has little or no influence on the position (i.e. an s-factor close to zero). Furthermore, it could even be possible that multiple satellites are affected by known ionospheric differences, but the current geometry causes the range domain errors to cancel out when projected into the position domain, leading to no significant positioning error.

RESULTS AND DISCUSSION

After introducing all refinements to the ionospheric monitoring concept, we will show results for the three major updates in the following sections. For simplification we show all results in this section only for the vertical domain. Typically, in vertical the uncertainly is larger while alert limits are tighter, making this the limiting factor. Nevertheless, the proposed monitoring would have to take place as well for the horizontal domain in an operational system.

Comparison of Test Statistic and Ionospheric Delay Difference

In this first evaluation we compare the refined test statistic using median removal with the previous approach when an increasing number of satellites experiences a known ionospheric delay difference. In a dual constellation scenario with 16 visible satellites, we

artificially introduce additional ionospheric delays at the airborne user. As previously introduced, the test statistics (equation (3)) to monitor for harmful impacts on the position solution should follow those delay differences as close as possible.
Figure 2 shows a comparison of the new monitoring scheme (median removal) on the right, with the old monitoring scheme (mean removal) on the left. The x-axis shows the time, while the y-axis refers to the test statistic for both methods. At times 2300, 2440, 2580 and 2720 seconds into the simulation an artificial jump in the ionospheric delay is introduced on four satellites to illustrate the effect on the test statistic. While in reality no such jumps would occur, this trivial example was chosen for simplicity and visual comparability of the results. Having no transient behavior, the estimation itself is not impacted by the sudden jumps in both cases.
Looking at the right plot in *Figure 2* we can find that the test statistics for the 4 impacted satellites (PRN 4, 6 and 16 from GPS and PRN 71/E01 from Galileo) follow the known introduced delay (dashed lines) quite well. Other satellites are not affected as long as fewer than half of the constellation experience the gradient. On the left side the situation is different. Even though for 1-2 affected satellites the impact is still clearly visible we can already see how the mean removal steps "spread" the gradient into other satellites and shifting all their test statistics, making it increasingly hard to identify the actually impacted satellites and affecting the performance of the monitor in general, as all satellites show increased test statistics, and not only the affected ones. Too many affected satellites could make it almost impossible to assess which satellite actually causes a problem in case of the mean removal.

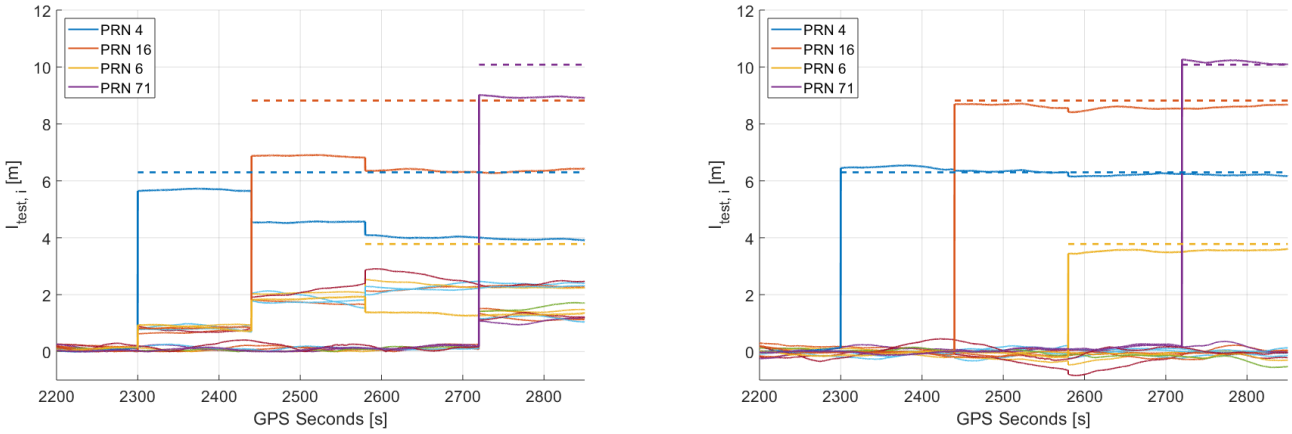

Figure 2 Comparison of test statistic per satellite with mean (left) and median removal (right). The dashed lines indicate the introduced additional ionospheric delay at the airborne user.

Regardless of how the monitoring is performed in the end, either in range domain as previously suggested or in position domain as proposed in this work, this improvement on the bias characterization of the test statistics brings a benefit already. Especially in situations where multiple satellites are affected by a gradient, the new approach can be more robust in identifying and excluding the affected satellites.

Potential for Full Constellation Monitoring

As new monitoring and exclusion strategy, we proposed to perform a monitoring of all currently used satellites at once. To assess the feasibility of this approach, we first take a look at the monitoring noise (equation (14)) as main driver of the combined test statistic in a nominal scenario without ionospheric activity.

$$6.1 \cdot \sqrt{\sum_{i=1}^{N} \sigma_{monitor,i}^2 \cdot s_{vert,i}^2} \tag{14}$$

In *Figure 3* we show the noise contribution over a 5 days simulation for 6 different scenarios. For a user in an equatorial latitude (Singapore) we simulate GPS and Galileo geometries based on almanac data (31 satellites GPS, 27 satellites Galileo) and using a 5° elevation mask. To derive $\sigma_{monitor,i}^2$ for the simulation, we use recently established dual frequency airborne models (see *Table 1*) and ground models based on two levels of ground station performance (Ground Accuracy Designators GAD-B and GAD-C [12]).

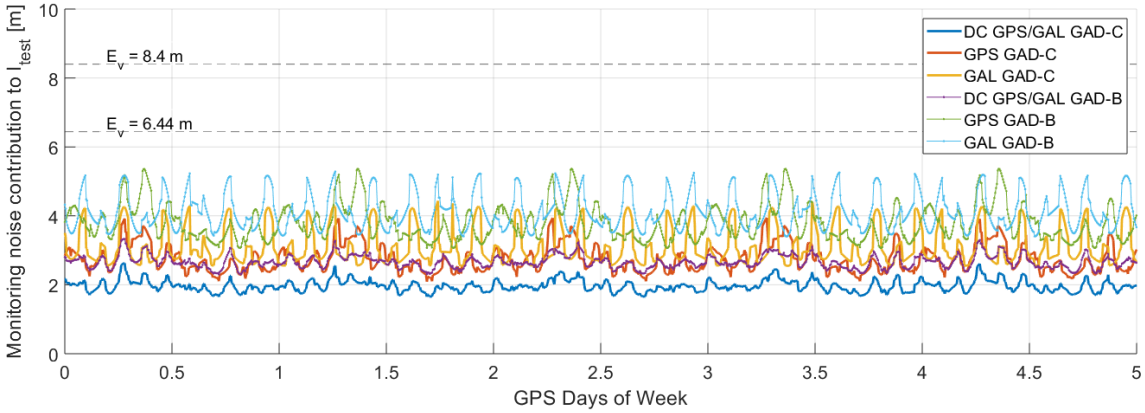

Figure 3 Nominal monitoring noise over time assuming GAD-B and GAD-C *[12]* ground stations performance and full dual constellation (GPS+GAL) and single constellation scenarios.

For reference we also depict typical values of $E_{v,iono}$ (6.44 m in case of a 2.5° Glide path angle and 8.4 m in case of 3°) as thresholds of interest in the figure.
In the optional situation of a GAD-C compliant GBAS station using two full constellations, we typically see values around 2 meters, combined monitoring noise. Downgrading to GAD-B still results in values below 3 meters most of the time. Looking at the single constellation results, values start to be significantly more dependent on the current geometry as expectable. Especially in case of a GAD-B station, values reach up to 5 meters, leaving little room towards the monitoring thresholds.

In a second step, we look closer at the case of dual constellation and GAD-C ground performance. Again, we perform simulations at an equatorial latitude using above mentioned setup and sigma models. Starting with all satellites in view, we arbitrarily pick 5 to 19 satellites. For each of this "random k out of all on view" cases we simulate 250,000 geometries distributed over a 10 days period. *Figure 4* shows the results in form of histograms (left) of the above-mentioned monitoring noise (equation (14)) and in terms of applicability of the all-in-view monitoring based on different monitoring thresholds (right).

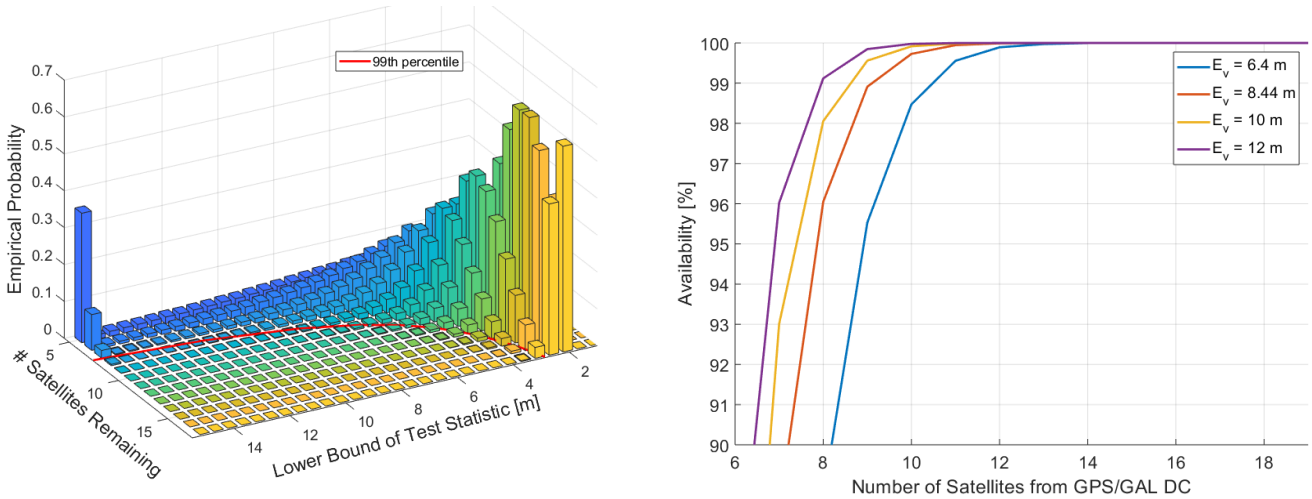

Figure 4 Lower Bound on test statistic in nominal conditions (left) and upper bound on applicability of all-in-view monitoring (right)

Looking at the histograms in *Figure 4* first we can find that especially below 9 satellites remaining we see a strong shift of the test statistic towards values above 10 meters and more. Above 10 satellites on the other hand, the 99th percentile of values decreased from

around 7.5 meters down to less than 3 meters. When comparing the resulting test statistics for all the different cases (number of selected satellites), we can additionally derive how likely an all-in-view monitoring is possible based on the nominal monitoring noise. This is depicted on the right side for 4 different thresholds ($E_{v,iono}$). In the most conservative case of 6.44 m we need at least 14 random satellites left to be able to monitor all satellites at once in 100% of all cases. For 8.4 this decreases to13 satellites and so forth for increasing thresholds.
This leads to the conclusion that the proposed all-in-view monitoring appears feasible in a dual constellation scenario even under the assumption that arbitrary (including worst case) satellites are unavailable. In single constellation scenarios on the other hand, depending on the final monitoring threshold and the nominal monitoring noise, this might lead to too many false alarms and therefore system unavailability.

Simulation of New Monitoring and Exclusion
As a last evaluation we show the behavior of the new proposed monitoring scheme along a simulated approach trajectory. For evaluating the monitor in a realistic but controlled ionospheric gradient scenario, we added a synthetic ionospheric gradient on top of simulated nominal GNSS data for a GBAS station with 4 reference receivers and an airborne user.

Simulated GNSS Data
The simulated nominal data used in this section was provided by Telespazio and INDRA Satnav in the framework of project SESAR 2020 PJ14-03-01. This nominal scenario comprises the GNSS signals simulated for four reference receivers situated at Barcelona airport. Simulated signals from 27 satellites are available for the GPS constellation and from 24 satellites (Walker configuration) for the Galileo constellation. Additionally, the simulated GNSS signals for an aircraft on a landing trajectory for Barcelona airport were included.

Residual Error Models
As previously mentioned, the residual errors included in the corrections (σ_{gnd}) and in the smoothed airborne pseudorange measurements (σ_{air}) per frequency and constellation have an impact on the monitor performance. The σ_{gnd} values depend on the installation of the GBAS ground station and are transmitted in the GBAS messages. For the evaluation of the airborne ionospheric monitor in this simulation, we used a conservative curve fitting of the σ_{gnd} values derived with data from Barcelona airport. The models used are summarized in Table 1.

σ_{gnd}	
Model GPS L1	$0.1148 \cdot e^{-0.0104 \cdot \theta}$
Model Galileo E1	$0.1172 \cdot e^{-0.01145 \cdot \theta}$
Model GPS L5	$0.1358 \cdot e^{-0.0242 \cdot \theta}$
Model Galileo E5a	$0.1242 \cdot e^{-0.1242 \cdot \theta}$

σ_{air}	
Model L1/E1	$0.13 + 0.17 \cdot e^{-\frac{\theta}{13}}$
Model L5/E5a	$0.11 + 0.18 \cdot e^{-\frac{\theta}{15}}$

Table 1 Used models for ground and airborne *[13]* noise and multipath for 100 s smoothing

Ionospheric Gradient Simulator
In a next step, an additional ionospheric delay is simulated and added over the nominal ionospheric delays present in each of the measurements (pseudoranges and carrier-phases in both frequencies). The synthetic delays are simulated in meters for L1 in the vertical domain. They are afterwards translated into the slant domain by multiplying with an obliquity factor (see equation 5.28 from [14]), which considers satellite elevations seen from the different receivers. The synthetic ionospheric delays are added consistently to both code and phase on both frequencies. For more details on how the ionospheric gradients are simulated and introduced into existing nominal data sets, refer to [15].
Figure 5 shows two snapshots of the simulated gradient travelling in the direction of flight of the aircraft. The trajectory of the aircraft is represented in grey and the yellow points represent the Ionospheric Pierce Points (IPPs) corresponding to the used set of 9 satellites. The parameters of the simulated gradient are the following: vertical slope of 100 mm/km, width of 100 km, speed of 750 m/s, and direction of 65° from the North pole (clockwise).

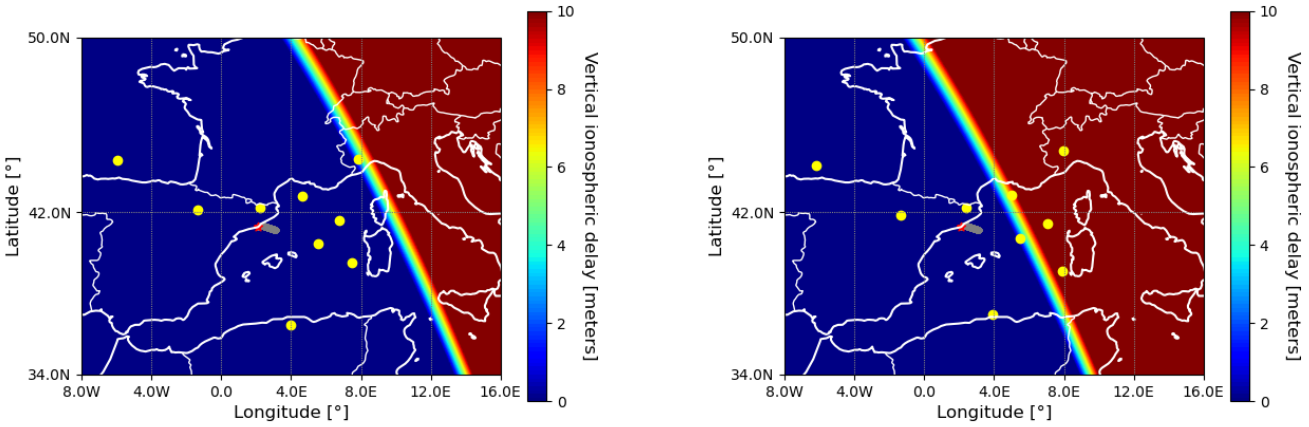

Figure 5 Visualization of the introduced gradient 10 minutes after the beginning of the simulated approach (left) and at the end of the approach (right). The yellow points show the IPPs as seen from the reference receiver 1 situated in Barcelona airport, the grey line shows the trajectory of the aircraft while on approach and the red point shows the airport.

Exemplary Simulation Results

In *Figure 6* we depict the behavior of the test statistic along the simulation. On the left we see the impact of each satellite in the position domain (i.e. $I_{test,i} \cdot s_{vert,i}$). The projected vertical error of PRN88 reaches its maximum when it is already affected by the gradient at the aircraft and starts to be affected at the ground (the maximum point is reached when I_{PRC} returns from the negative overshoot due to the smoothing filter characteristic). For PRN 88 s_{vert} is between 1.1 (beginning) and around 0.75 (end). Afterwards PRN 72 and PRN 7 are experiencing the gradient. While PRN 72 has a higher value for I_{test}, a low s_{vert} between -0.4 and -0.1 s_{vert} limits the impact on the position error. PRN 7 on the other hand with s_{vert} between 1.4 and 1 causes another visible spike.

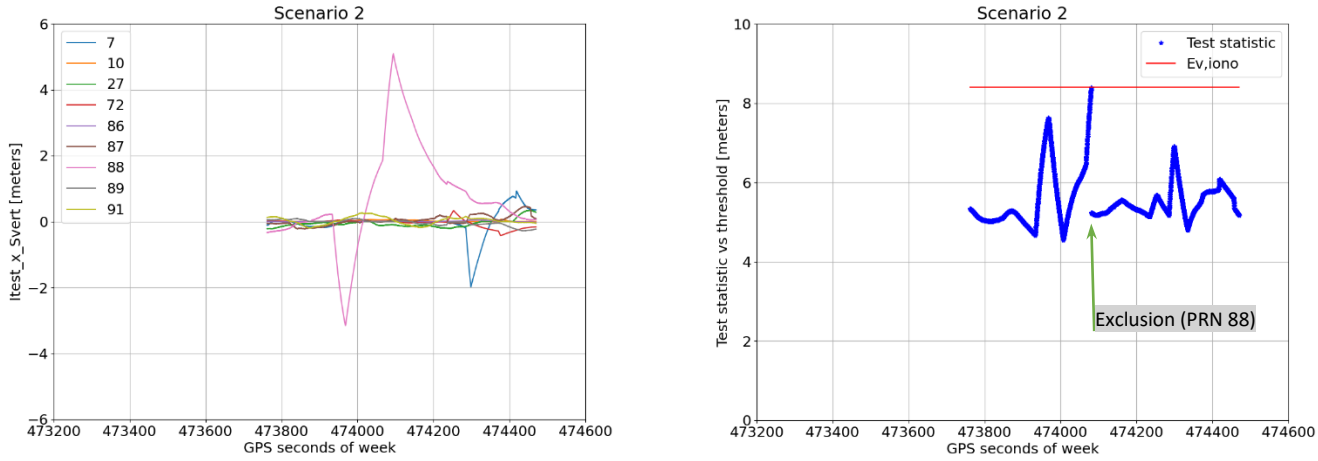

Figure 6 Projected vertical error of individual satellites (left) and combined test statistic with threshold (E_v) (right)

The right side of *Figure 6* shows the combined test statistic together with the applied threshold of 8.4 meters. The satellite excluded is PRN 88. After the exclusion, the test statistic almost returns to the "nominal" value around 5 meters until PRN72 (first small peak after 474200 GSW) and PRN7 (second bigger peak after 474200 GSW) are affected. Note that, even though up to four satellites

remain affected at the end of the simulation, their vertical position error contribution is low and therefore they are not excluded by the monitor. This becomes evident when looking at the vertical position errors in *Figure 7*.

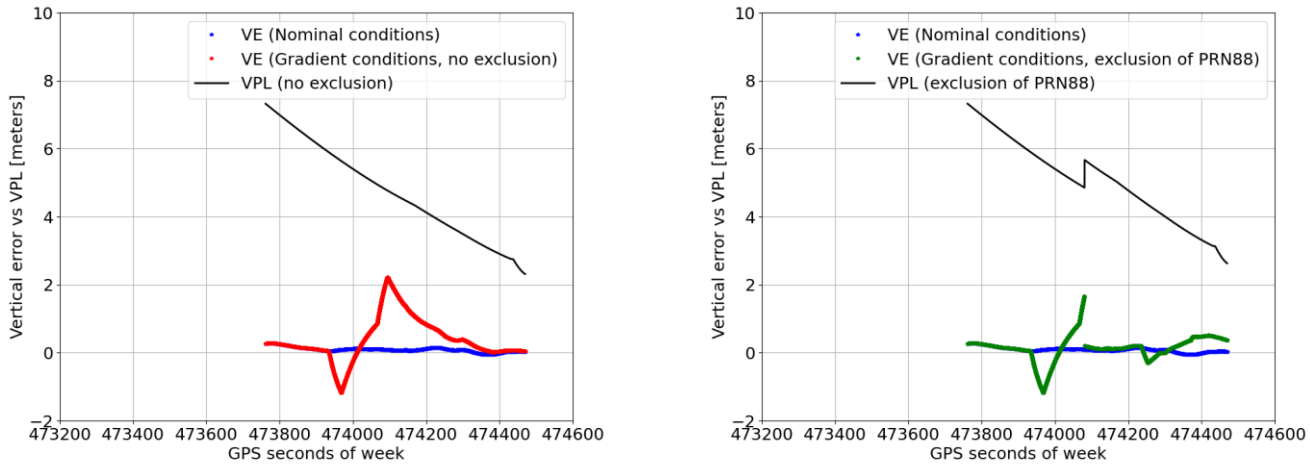

Figure 7 Vertical position error and protection level for simulated approach with (right) and without (left) exclusion according to ionospheric monitoring

Figure 7 compares the vertical protection level (VPL) and vertical position error for a simulation with and without the ionospheric monitoring in place. For this plot, the vertical error is derived from the known aircraft position during the simulation and the position calculated for single frequency L1/E1 processing using a 100 s smoothing time constant. On the left side, without exclusion, we can see the vertical errors grow up to almost 2.5 meters in comparison to the nominal scenario without the added gradient.
On the right side, with exclusion, the vertical error grows until about 1.75 meters before the monitoring threshold is reached and PRN 88 is excluded from the positioning. The position error afterwards returns almost back to the nominal value until the onset of the gradient to more satellites. In both cases, the vertical errors stay within the protection levels, indicating no integrity fault and highlighting as well the impact of having a strong geometry to be robust against ionospheric gradient threats.

CONCLUSIONS AND FUTURE WORK

In this paper we described several refinements to a previously developed concept for ionospheric monitoring in DFMC GBAS.
The presented updates on the monitoring imply:

- A better monitoring performance from the first affected satellites on due to the removal of biases in the test statistics due to the common ionospheric error previously included.
- A proof that all common biases on any of the contributors to the test statistic (like different set of satellites on the ground and in the airborne, different signal delays on L1/L5) are mitigated by the median removal and do not affect the monitoring
- A tighter bound on the expected monitoring noise in case of the monitoring multiple affected satellites at once
- A way to monitor the ionospheric threat for all used satellites at once with a single test and without any prior knowledge or assumptions on the number of affected satellites, depending on the actual noise levels and number of satellites in view.

In the next steps, the monitoring scheme will be applied to larger data sets from previous and ongoing flight measurement campaigns to assess the performance and applicability in with real measurements containing so far unmodelled effects [11]. Some of those should be bound by existing noise and multipath overbounds (σ_{air}), others need further studies. Especially errors introduced in the corrections due to the averaging process among multiple ground reference receivers as well as elevation and azimuth dependent antenna ground delay variations are to be mentioned here, which can affect the ionospheric estimates both on the airborne and ground side. Studies shall furthermore assess whether those effects have a significant effect on the monitoring and require further adaptions of the threshold or additional modelling of antenna parameters.

ACKNOWLEDGMENTS
The authors would like to thank INDRA Satnav and Telespazio for providing the simulated nominal data in the frame of the European project SESAR 2020 PJ14-03-01.

REFERENCES

[1] S. Pullen, Y. S. Park and P. Enge, "Impact and mitigation of ionospheric anomalies on ground-based augmentation of GNSS," *Radio Science,* vol. vol. 44, no. 1, pp. 1-10, 2009.

[2] C. Mayer, B. Belabbas, M. Jakowski, M. Meurer and W. Dunkel, "Ionosphere Threat Space Model Assessment for GBAS," in *Proceedings of the 22nd International Technical Meeting of the Satellite Division of The Institute of Navigation (ION GNSS 2009)*, Savannah, GA, 2009.

[3] M. Kim, Y. Choi, H.-S. Jun and J. Lee, "GBAS ionospheric threat model assessment for category I operation in the Korean region," *GPS Solutions,* vol. 19, no. 3, p. 443–456, 2015.

[4] D. Gerbeth, M.-S. Circiu, M. Caamano and M. Felux, "Nominal performance of future dual frequency dual constellation GBAS," *International Journal of Aerospace Engineering,* 2016.

[5] M. Felux, M.-S. Circiu, J. Lee and F. Holzapfel, "Ionospheric gradient threat mitigation in future dual frequency GBAS," *International Journal of Aerospace Engineering,* p. 10, 2017.

[6] M. Felux, M.-S. Circiu, D. Gerbeth and M. Caamano, "Experimental Validation of an Ionospheric Monitoring Scheme for Dual Frequency GBAS," in *Proceedings of the 29th International Technical Meeting of the Satellite Division of The Institute of Navigation (ION GNSS+ 2016)*, Portland, Oregon, 2016.

[7] M. Stanisak, A. Lipp and T. Feuerle, "Possible VDB formatting for multi-constellation/multi-frequency GBAS services.," in *Proceedings of the 28th International Technical Meeting of the Satellite Division of The Institute of Navigation (ION GNSS+ 2015)*, Tampa, Florida, 2015.

[8] M. Felux, M.-S. Circiu, D. Gerbeth, M. Caamano and M. Stanisak, "Ionospheric monitoring in a dual frequency GBAS," in *2016 IEEE Aerospace Conference, 2016*, Big Sky, Montana, 2016.

[9] N. C. Schwertman, A. J. Gilks and J. B. Cameron, "A Simple Noncalculus Proof That the Median Minimizes the Sum of the Absolute Deviations," *The American Statistician,* pp. 38-39, 1990.

[10] RTCA DO-253D, "Minimum Operational Performance Standards for GPS Local Area Augmentation System Airborne," 1, June 27, 2019.

[11] T. Murphy, M. Harris, G. McGraw, J. Wichgers, L. Lavik, M. Topland, M. Tuffaha and S. Saito, "Alternative Architecture for Dual Frequency Multi-Constellation GBAS," in *Proceedings of the 34th International Technical Meeting of the Satellite Division of The Institute of Navigation (ION GNSS+ 2021)*, St. Louis, Missouri, 2021.

[12] EUROCAE, "ED-114B "MOPS For Global Navigation Satellite Ground Based Augmentation System Ground Equipment To Support Precision Approach and Landing"," 2019.

[13] M.-S. Circiu, S. Caizzone, C. Enneking, F. Fohlmeister, M. Rippl, M. Meurer, M. Felux, I. Gulie, D. Rüegg, J. Griggs, R. Lazzerini, F. Hagemann, F. Tranchet, P. Bouniol and M. Sgammini, "Final Results on Airborne Multipath Models for Dualconstellation Dual-frequency Aviation Applications," in *Proceedings of the 2021 International Technical Meeting of The Institute of Navigation*, 2021.

[14] P. Misra and P. Enge, Global Positioning System: Signals, Measurements, and Performance, Ganga-Jamuna Press, 2006.

[15] M. Caamano, J. M. Juan, M. Felux, D. Gerbeth, G. González-Casado and J. Sanz, "Network-based ionospheric gradient monitoring to support GBAS," *NAVIGATION, Journal of the Institute of Navigation*, vol. 68, no. 1, pp. 135-156, 2021.